Research Square

Preprints are preliminary reports that have not undergone peer review.
They should not be considered conclusive, used to inform clinical practice,
or referenced by the media as validated information.

Helium Plasma-Activated Medium Promotes a Regeneration-Associated Functional and Transcriptional Response in Hair Follicle Stem Cells

Kamal Hajisharifi

hajisharifi@khu.ac.ir

Kharazmi University

Sara Emadi

Kharazmi University

Elaheh Amini

Kharazmi University

Hassan Mehdian

Kharazmi University

Sareh Pandamooz

Shiraz University

Erfan Tamandeh

Kharazmi University

Eric Robert

UMR 7344 GREMI, CNRS/Université d'Orléans

Article

Keywords: cold atmospheric plasma, plasma-activated medium, hair follicle stem cells, gene expression, regeneration, wound healing

Posted Date: November 24th, 2026

DOI: https://doi.org/10.21203/rs.3.rs-11613897/v1

License: This work is licensed under a Creative Commons Attribution 4.0 International License.
Read Full License

Additional Declarations: No competing interests reported.

Abstract

Hair follicle stem cells (HFSCs) are central regulators of hair follicle regeneration and tissue repair, requiring coordinated control of stem-cell activation, migratory responsiveness, and epithelial plasticity. Plasma-activated media have emerged as promising bioactive platforms for regenerative applications through the controlled delivery of reactive oxygen and nitrogen species. In this study, the biological effects of helium plasma-activated medium (He-PAM) on HFSCs were evaluated using functional and molecular analyses. Cell metabolic and migratory activity were assessed alongside the expression of genes associated with regenerative activation (*Runx1, Lgr4*, and *Ccnd1*), migratory competence (*Cxcr4*), and epithelial plasticity (*Snai1* and *Ovol2*). The selected He-PAM significantly enhanced HFSCs metabolic activity and migration while inducing coordinated transcriptional changes across the investigated biological processes. Increased expression of *Runx1, Lgr4*, and *Ccnd1* was associated with regenerative activation, *Cxcr4* upregulation was consistent with the enhanced migratory response observed in the scratch assay, and the concurrent induction of *Snai1* and *Ovol2* was consistent with a transcriptional pattern associated with epithelial plasticity. Collectively, these findings indicate that He-PAM promotes a regeneration-associated functional and transcriptional response in HFSCs, characterized by enhanced metabolic and migratory activity together with coordinated changes in genes associated with regenerative activation, migratory competence, and epithelial plasticity. These findings support the potential of He-PAM as a plasma-based approach for modulating cellular processes relevant to hair follicle regeneration and regenerative medicine.

1. Introduction

Hair follicle stem cells (HFSCs), localized within the bulge region of the hair follicle, are responsible for follicular cycling, epidermal repair, and neuroectodermal regeneration [1, 2]. Owing to their self-renewal capacity and multipotency, HFSCs represent an attractive cellular source for regenerative medicine, especially for alopecia treatment and cutaneous wound repair [3, 4]. Hair follicle-derived stem cell populations have also been investigated for their potential applications in cell-based regenerative therapies [5].

Recent advances in hair follicle biology have substantially expanded the understanding of the mechanisms governing the function of HFSCs during tissue homeostasis and regeneration. Emerging evidence indicates that effective follicular regeneration is not solely dependent on stem-cell proliferation, but rather requires the coordinated integration of multiple biological processes that collectively determine regenerative competence. Among these, activation of stem-cell regenerative programs is considered a prerequisite for hair-cycle re-entry and long-term follicular renewal, enabling HFSCs to transition from a quiescent state toward active participation in tissue regeneration [6, 7]. In parallel, the acquisition of migratory competence has emerged as a critical determinant of regenerative efficacy, as HFSCs must respond to environmental cues, relocate within damaged tissues, and contribute to wound repair and follicular reconstruction [8]. Furthermore, recent studies have highlighted epithelial plasticity as a fundamental feature of regenerative stem cells, allowing HFSCs to dynamically adapt their cellular

state in response to niche-derived signals while preserving their regenerative identity. Controlled transitions between epithelial and mesenchymal programs are now recognized as essential mechanisms underlying tissue remodeling, wound re-epithelialization, and successful follicular regeneration [9–11]. Collectively, these observations suggest that simultaneous evaluation of regenerative activation, migratory potential, and epithelial plasticity provides a biologically relevant framework for assessing cellular processes associated with regenerative competence in HFSCs and may offer valuable insight into the mechanisms through which emerging therapeutic interventions influence hair follicle regeneration.

Cold atmospheric plasma (CAP), a partially ionized gas near room temperature, generates a complex mixture of electrons, ions, UV photons, reactive oxygen and nitrogen species (RONS), and physical factors including transient electric fields, electromagnetic fields, charged species, and plasma-induced microcurrents, all of which contribute to biological responses [12–15]. Recent evidence indicates that CAP-induced biological responses arise from the interplay between RONS and these physical plasma components [14, 15]. When CAP interacts with liquids, it generates plasma-activated medium (PAM), containing bioactive reactive species capable of modulating cellular signaling pathways. Plasma-based treatments have been reported to influence PI3K/AKT and MAPK signaling pathways involved in cellular responses relevant to tissue repair [16, 17]. Moreover, experimental evidence suggests that the response to CAP can be influenced by the epithelial–mesenchymal state of cells, indicating that plasma-induced biological effects may depend on cellular phenotype and context [18]. Consistent with this context-dependent activity, PAM has been shown to modulate keratinocyte responses relevant to tissue repair [19]. In hair follicle biology, Runx1 contributes to stem-cell activation and proliferation [20], whereas dermal papilla cells provide regulatory signals that influence follicular activity and respond to plasma stimulation through Wnt/β-catenin-associated signaling [21]. Lgr4 is another important regulator of hair follicle stem-cell activation and hair-cycle progression [22]. Beyond these cell-specific responses, CAP has also been reported to influence wound repair and extracellular matrix-associated processes [23]. Furthermore, plasma-induced β-catenin signaling has been associated with enhanced dermal papilla cell proliferation, providing additional evidence that plasma-based interventions can influence cellular pathways relevant to hair follicle biology [24].

Despite growing evidence supporting their regenerative potential in various cell types and tissues, how plasma-derived reactive species influence cellular processes associated with regenerative competence in hair follicle stem cells (HFSCs) remains insufficiently understood. We therefore hypothesized that He-PAM could modulate regeneration-associated cellular responses in HFSCs through coordinated effects on cellular activity, migration, and the expression of genes associated with regenerative activation and epithelial plasticity. The present in vitro study therefore aimed to determine whether He-PAM can promote regeneration-associated functional and transcriptional responses in HFSCs. To address this hypothesis, cellular metabolic and migratory activity were evaluated in parallel with the expression of genes associated with stem-cell recruitment and migratory responsiveness (*Cxcr4*), epithelial plasticity and dynamic cell-state transitions (*Snai1* and *Ovol2*), and regenerative activation pathways implicated in stem-cell competence, follicular renewal, and hair-cycle regulation (*Runx1, Lgr4*, and *Ccnd1*). By

integrating functional and transcriptional analyses, this study was designed to define the cellular response of HFSCs to He-PAM and to assess whether these responses are consistent with biological processes associated with hair follicle regeneration.

2. Materials and Methods

2.1. Plasma Jet Fabrication and PAM Preparation

A custom-designed helium CAP jet consisted of a stainless-steel pin electrode (0.3 mm diameter, 15 cm length) coaxially aligned inside a quartz tube (ID 3 mm, OD 5 mm) with a copper ring electrode (5 mm width) near the outlet (Fig. 1) was used in this work. A sinusoidal voltage signal (9–14 kV, 14 kHz) was applied across the electrodes while helium flow was set at 1 slm. The distance between the tube nozzle and the liquid surface was fixed at 15 mm. To prepare PAM, 600 μL of serum-free α-MEM was exposed to CAP for 30 or 60 s and used within 30 min. Treatment conditions are summarized in Table 1.

Table 1
Voltage and duration conditions used for PAM preparation.

Time (s)	Voltage (kV)	Group ID
0	0	Control
30	9	t1
60	9	t2
30	10	t3
60	10	t4
30	11	t5
60	11	t6
30	12	t7
60	12	t8
30	13	t9
60	13	t10
30	14	t11
60	14	t12

2.2. Isolation and Culture of Hair Follicle Bulge-Derived Stem/Progenitor Cells and Study Design

Nestin-expressing hair follicle bulge-derived stem/progenitor cells were isolated from the vibrissal bulge region of three-week-old male Wistar rats (30–35 g) obtained from the Animal House of Kharazmi University, Tehran, Iran, using the established bulge-explant isolation and culture approach previously described and characterized by our research group [25, 26]. The cells were isolated from whisker-pad tissues collected post-mortem from rats that had been euthanized by carbon dioxide (CO_2) inhalation for purposes unrelated to the present study. No chemical anesthetic was administered prior to euthanasia. Briefly, whisker pads were excised under sterile conditions, disinfected with 70% ethanol, and subsequently immersed in povidone–iodine (Betadine) solution for 3–5 min. Individual vibrissal follicles were then carefully dissected under a stereomicroscope, and the bulge regions were isolated using fine microsurgical needles. The explanted bulges were cultured on collagen type I–coated dishes (1 mg/mL, Roche; #11179179001) in α-minimum essential medium (α-MEM) supplemented with 10% fetal bovine serum (FBS) and 10% chick embryo extract (CEE) and 1% penicillin/streptomycin (P/S). Cultures were maintained at 37°C in a humidified cell culture incubator containing 5% CO_2. Migratory cells emerged from the explants within 3–4 days and were expanded to passage 4 prior to experimental use. For each isolation procedure, vibrissal bulge explants were obtained from three rats, and the cells migrating from these explants were pooled and expanded in culture. This isolation procedure was independently repeated three times, involving a total of nine rats. The cell populations obtained from the three isolation procedures were subsequently combined and expanded as a common cell population for the experimental assays. The isolation and culture procedure is schematically illustrated in Fig. 2. All procedures involving the source animals and the collection of post-mortem tissues were performed in accordance with relevant institutional guidelines and regulations.

2.3. Immunofluorescence Staining

To assess cellular morphology and cytoskeletal organization and to confirm Nestin expression in cultured bulge-derived stem/progenitor cells, F-actin staining and Nestin immunostaining were performed separately on different cell preparations. HFSCs were seeded onto four-chamber glass slides at a density of 7.5×10^4 cells per chamber and cultured overnight. Cells were then fixed with 4% paraformaldehyde (PFA) for 10 min at room temperature and washed three times with PBS containing 0.1% Tween-20 (PBS-T). Subsequently, cells were blocked for 30 min at room temperature with blocking solution containing 0.1% Triton X-100, 1% fetal bovine serum (FBS), and 10% normal goat serum in PBS. For assessment of cellular morphology and cytoskeletal organization, one set of cells was incubated with Alexa Fluor™ 488-conjugated phalloidin (1:200; Cell Signaling Technology, #8878) diluted in blocking solution for 1 h. For Nestin immunostaining, separate cell preparations were incubated overnight at 4°C with mouse anti-Nestin monoclonal antibody (1:50; Abcam, #ab6142). Next day, after three washes with PBS-T, cells were incubated with goat anti-mouse IgG Alexa Fluor™ 488 (1:1000; Thermo Fisher Scientific, #A-11001) for 2 h at room temperature. Cell nuclei were counterstained using ProLong™ Glass Antifade Mountant with NucBlue™ Stain (Invitrogen, #P36985), and coverslips were mounted prior to imaging. Fluorescence images were acquired using a Leica DM5000B epifluorescence microscope.

2.4. Cell Treatment and Metabolic Activity Assay

Approximately 1×10^4 cells per well were seeded into 96-well plates and incubated overnight to allow cell attachment. The culture medium was then replaced with 100 µL of freshly prepared PAM generated under different applied voltages and plasma exposure durations. Control wells received untreated α-MEM. Briefly, cells were incubated with MTT solution (5 mg/mL; Sigma Aldrich, USA; cat number: CT01/CT02) for 3 h at 37°C, after which the resulting formazan crystals were quantified by measuring the absorbance at 570 nm using a microplate reader (Bio-Rad, USA).

2.5. Scratch Migration Assay

HFSCs were cultured in 6-well plates until they reached approximately 85% confluence. The confluent monolayers were incubated with Mitomycin C (concentration of 5 µg/mL; Stemcell Technologies, Canada; cat number: 73274 100–1048) for 2 h at 37°C (Mouritzen and Jenssen 2018). After aspiration, the confluent monolayers were scratched with a sterile tip and rinsed with PBS. In order to assess migratory capacity, the cells were incubated with PAM prepared under five selected He-PAM conditions (Table 2), chosen based on metabolic activity profiles (12–14 kV, 30–60 s). Wound-closure images were captured at 0 h and 48 h using an inverted microscope. Wound area was quantified using ImageJ software at 0 and 48 h, and the percentage of wound closure was calculated using the following formula:

Wound Closure (%) = [(wound area immediately after scratching (0 h)− wound area after 48h) / (wound area immediately after scratching (0 h))] × 100

For comparison among treatment groups, wound-closure values were subsequently normalized to the untreated control group, which was set to 100%, and expressed as relative wound closure (% of control).

Table 2
PAM treatment conditions selected for migration and gene-expression assays.

Time (s)	Voltage (kV)	Group ID
0	0	Control
30	12	t7
60	12	t8
30	13	t9
60	13	t10
30	14	t11

2.6. Quantitative Real-Time PCR (qRT-PCR)

Total RNA from treated and untreated HFSCs was extracted using a RNeasy Kits for RNA Purification kit (Qiagen; Cat. No.: 74104) according to the manufacturer's instructions. Complementary DNA (cDNA) was synthesized using the First Strand Reverse Transcription Kit (Qiagen, Cat. No.: 205311). Expression levels of *Snai1*, *Cxcr4, Ovol2, Runx1*, *Lgr4*, and *Ccnd1* were quantified by real-time PCR. In this regard, 10

μL SYBR green mastermix,1 μL of forward primer, 1 μL of reverse primer, 1 μL cDNA, and 7 μL DEPC-treated water were mixed in 20 μL total volume and PCR reactions were performed in triplicate using a CFX-96 Real-Time PCR System (Bio-Rad, USA). *Gapdh* was used as the internal reference gene. The primer sequences for the target and reference genes are listed in Table 3. The PCR cycling conditions were as follows: initial denaturation at 95°C for 3 min, followed by 45 cycles at 95°C for 10 seconds, annealing degree for 30 seconds and extension time for 20 seconds. The target gene expression level was calculated using the $2^{-\Delta\Delta CT}$ formula.

Table 3
Primer sequences used for qRT-PCR analysis of target genes in HFSCs.

Gene ID	Primer Seq (5'->3')	Tm	PCR Product (bp)
Snai1	AGTTGTCTACCGACCTTGCG	60.04	128
snail family transcriptional repressor 1	TGCAGCTCGCTATAGTTGGG	59.95	
Cxcr4	GGCGTTTGGTGCTCCGGTA	62.89	206
C-X-C motif chemokine receptor 4	TTGCCCACTATGCCAGTCAAG	60.61	
Ovol2	CGAGTAGCCGGGAGTGAAGG	62.01	192
ovo-like zinc finger 2	AGACTTTGGGCATGGTGGGA	61.43	
Runx1	CGGGACCGTTTGTAATAGCC	58.71	121
RUNX family transcription factor 1	GTTAGCAACTGGCCGCTTAG	59.27	
Lgr4	ACCAGGGTGTTTGTGAGAACCC	62.67	93
leucine-rich repeat-containing G	AACCGCACGGCTCCTCAAG	62.88	
Ccnd1	CAAGTGTGACCCGGACTGC	60.96	209
cyclin D1	TACTTGGTGACTCCCGCCT	60.23	

2.7. Statistical analysis

Cells obtained from three independent primary isolation procedures were combined to establish a common cell population for subsequent experiments. All experiments were performed in three separate experimental runs using this shared cell population under the same culture and treatment conditions. Data are presented as mean ± SD of the three experimental runs (n = 3). These experimental runs do not represent independent biological replicates derived from separate cell isolations. Data were analyzed using one-way ANOVA followed by Tukey's post hoc test. A p value of less than 0.05 was considered statistically significant.

3. Results

3.1. Morphological Assessment and Nestin Expression of Hair Follicle Bulge-Derived Stem/Progenitor Cells

Hair follicle bulge-derived stem/progenitor cells were isolated from the bulge region of rat vibrissal follicles using the explant approach described in Section 2.2 (Fig. 3A,B). Our previous studies using this isolation approach reported immunophenotypic characterization of the resulting bulge-derived stem/progenitor cells, including Nestin and SOX10 immunostaining [25, 26]. Following culture, the cells exhibited a typical spindle-shaped, fibroblast-like morphology and formed a homogeneous adherent cell population (Fig. 3C). To further characterize the cultured cells, phalloidin staining revealed a well-organized filamentous actin (F-actin) cytoskeleton (Fig. 3D), while Hoechst staining demonstrated uniformly distributed nuclei (Fig. 3D'). The merged image confirmed the elongated morphology and intact cytoskeletal organization of the cultured cells (Fig. 3D''). Immunofluorescence analysis demonstrated Nestin expression in the cultured cells (Fig. 3E). Hoechst staining identified the cell nuclei (Fig. 3E'), and the merged image (Fig. 3E'') confirmed Nestin immunoreactivity in the majority of cultured cells. The observed Nestin immunoreactivity was consistent with previous reports of Nestin-expressing stem/progenitor cells derived from rat vibrissal bulge explants [25, 26].

3.2. Cell metabolic activity

As shown in Fig. 4, most PAM-treated cells showed no significant cytotoxicity 24 h after treatment. Among the treatment groups, cells exposed to 11kV for 30s and 13 kV for 30s exhibited reduced HFSC metabolic activity (86.6%, 76.7%; *$p < 0.05$). Meanwhile, PAM treatments increased cell metabolic activity compared with the control group 48 h after treatment. Based on the MTT assay findings, the maximum HFSC metabolic activity was observed following exposure to 14 kV for 30s and 11 kV for 60s, reaching 151.3 and 151.9% of the control value, respectively (***$p < 0.001$). Statistical analysis confirmed significant differences among groups ($F = 4.70$, (***$p < 0.001$). In contrast, HFSC metabolic activity decreased to 90.2% following exposure to 13 kV for 60s (48h post treatment). Overall, these findings indicate a time- and parameter-dependent metabolic response to He-PAM, with selected treatment conditions enhancing metabolic activity at 48 h rather than a uniform increase across all plasma settings.

3.3. Scratch assay

Representative scratch-assay images showed that He-PAM treatment promoted the migratory behavior of HFSCs. Microscopic images indicated that the degree of wound closure in t8 (12 kV, 60s) and t11 (14 kV, 30s) treatment groups after the scratch (0 hour) and 48 hours PAM exposure was higher than that observed in the t7, t9, t10 experimental groups (Fig. 5A). Quantitative analysis using ImageJ revealed a parameter-dependent enhancement of wound closure following He-PAM treatment. After 48 h, the actual wound-closure percentages were 59.8% in the untreated control, 82.6% in t8 (12 kV, 60 s), and 92.4% in t11 (14 kV, 30 s). When normalized to the untreated control (100%), these values corresponded to

approximately 138% and 155% relative wound closure for t8 and t11, respectively (Fig. 5B). The t7 condition also showed an increase in relative wound closure, whereas t9 and t10 produced comparatively smaller responses. These findings indicate that the migratory response to He-PAM depended on the plasma-treatment parameters rather than increasing uniformly with voltage or exposure duration.

.

3.4. He-PAM Induces Coordinated Changes in Regeneration-Associated Gene Expression

To investigate the transcriptional responses associated with regenerative activation, migration, and epithelial plasticity, the expression of six functionally relevant genes was examined following He-PAM treatment. *Runx1, Lgr4*, and *Ccnd1* were evaluated in relation to stem/progenitor activation and proliferative competence, *Cxcr4* as a marker associated with migratory responsiveness, and *Snai1* and *Ovol2* as regulators associated with epithelial plasticity. As exhibited in Fig. 6, under exposure with Helium-PAM (t7, t8, t9, t10, t11) the expression of target genes changed compared with control. Among the investigated conditions, t11 (14 kV, 30 s) produced one of the most pronounced overall transcriptional responses, including the highest expression of *Cxcr4*, *Snai1*, *Ovol2*, *Lgr4*, and *Ccnd1*. The highest level of gene expression was observed for Cxcr4 (5.86-fold change). Additionally, *Ovol2* and *Lgr4* gene expression indicated 2.29-fold change, and 1.46-fold change, respectively 48h post treatment with t11. Together, these changes indicate a coordinated transcriptional response involving genes associated with stem/progenitor activation and proliferative competence. In this regard, the lowest degree of upregulation was observed for *Lgr4* expression level under exposure with t11. In addition, *Snai1* and *Ccnd1* expression levels increased by 2.38-fold and 3.73-fold, respectively, following treatment with He-PAM at 14 kV for 30 s. These transcriptional changes indicate that the He-PAM response extends beyond genes associated with cell-cycle regulation and includes genes related to migratory responsiveness and epithelial plasticity. These transcriptional changes are consistent with modulation of genes associated with epithelial plasticity and Wnt-related regenerative regulation in HFSCs treated 14 kV, 30s Helium-PAM jet (Fig. 6). Fold changes are summarized in Table 4.

Table 4
Fold-change expression of target genes in HFSCs after PAM treatment.

Group	*Snai1*	*Cxcr4*	*Ovol2*	*Runx1*	*Lgr4*	Ccnd1
Control	1.000	1.000	1.000	1.000	*1.000*	1.000
t7	1.803	3.183	1.866	1.932	*1.231*	2.549
t8	2.071	3.249	2.219	1.803	*1.320*	3.605
t9	1.682	2.828	2.000	1.569	*1.315*	2.639
t10	1.366	2.219	1.366	1.066	*1.072*	2.07
t11	2.378	5.856	2.297	1.414	*1.464*	3.732

Collectively, the qPCR findings demonstrate that He-PAM induces coordinated transcriptional changes in genes associated with stem/progenitor activation, migratory responsiveness, and epithelial plasticity. Together with the observed increases in metabolic and migratory activity, these findings define a functional and transcriptional response consistent with regeneration-associated cellular processes.

4. Discussion

This study demonstrates that He-PAM elicits a coordinated functional and transcriptional response in HFSCs, characterized by increased metabolic activity and migration together with changes in genes associated with regenerative activation, migratory responsiveness, and epithelial plasticity. Collectively, these findings identify a regeneration-associated cellular response rather than providing direct evidence of follicular regeneration.

Among the investigated conditions, He-PAM generated at 14 kV for 30 s showed one of the most consistent combined functional and transcriptional responses, suggesting that the biological effects of plasma-derived reactive species are highly dependent on treatment parameters. This observation is consistent with the growing concept of plasma-induced hormesis, whereby low and controlled levels of reactive oxygen and nitrogen species (RONS) function as signaling mediators that stimulate adaptive cellular responses, whereas excessive oxidative stimulation may compromise cellular function and survival. The variability observed among the different He-PAM conditions, including the absence of comparable metabolic or migratory enhancement under some treatment conditions, indicates a non-monotonic and parameter-dependent cellular response to He-PAM. Such variability may reflect differences in the physicochemical composition and effective reactive-species dose generated under different plasma conditions; however, because He-PAM composition was not directly characterized in the present study, the mechanisms underlying these condition-specific responses cannot be determined from the current data. In the context of HFSCs biology, successful regeneration requires not only maintenance of cell survival but also activation of molecular programs that enable stem cells to respond effectively to regenerative cues and participate in tissue renewal. Consistent with this concept, the

increased metabolic activity observed following selected He-PAM treatment was accompanied by elevated expression of *Runx1*, *Lgr4*, and *Ccnd1*, genes that have been implicated in stem-cell competence, follicular regeneration, and hair-cycle re-entry [27–29]. Importantly, recent advances in HFSCs biology have increasingly emphasized that regenerative competence is governed by dynamic interactions between stem cells and their niche rather than by proliferative activity alone, highlighting the importance of stem-cell activation programs during tissue regeneration [6, 7]. Collectively, these findings suggest that selected He-PAM conditions promote a functional and transcriptional response associated with enhanced stem/progenitor activation and regenerative competence.

Beyond its effects on metabolic activity, the selected He-PAM significantly enhanced HFSC migration, providing functional evidence of a cellular response relevant to regenerative processes. This functional observation was accompanied by a pronounced upregulation of *Cxcr4*, which represented the most strongly induced gene in the present study. CXCR4-mediated signaling plays a central role in stem-cell homing, chemotaxis, wound healing, and tissue regeneration through cellular responses to CXCL12 gradients [8, 30]. Therefore, the substantial increase in *Cxcr4* expression, together with the enhanced wound-closure rate observed in the scratch assay, supports a coordinated response involving enhanced migratory activity and the expression of a key migration-associated signaling receptor. Previous studies have suggested that plasma-derived reactive species may influence redox-sensitive signaling networks, including PI3K/AKT, NF-κB, and TGF-β-associated pathways [13, 18]. Although these signaling cascades were not directly evaluated in the present study, the observed transcriptional and functional responses are consistent with the possibility that selected He-PAM modulates downstream pathways involved in cellular motility and regeneration-associated cellular responses. Since effective tissue regeneration depends on the ability of stem/progenitor cells to sense, migrate toward, and respond to regenerative microenvironments, the enhanced migratory response observed following He-PAM exposure may represent a functionally relevant feature of the regeneration-associated cellular response identified in this study.

An additional and particularly noteworthy finding of this study was the simultaneous upregulation of *Snai1* and *Ovol2*. Traditionally, SNAI1 is recognized as a key regulator of epithelial-to-mesenchymal transition (EMT), promoting transient cellular motility and cytoskeletal remodeling required for tissue repair and re-epithelialization [31, 32]. In contrast, OVOL2 functions as an important regulator of mesenchymal-to-epithelial transition (MET) and contributes to the restoration of epithelial identity following regenerative remodeling [9, 33]. The concurrent induction of both factors does not support a simple interpretation of a unidirectional EMT response and is instead consistent with a transcriptional program associated with epithelial plasticity. Recent studies have increasingly recognized that successful tissue regeneration depends on dynamic and reversible epithelial–mesenchymal state transitions that allow stem cells to adapt to regenerative demands while preserving their long-term regenerative identity [9, 11, 33–36]. Therefore, the coordinated elevation of *Snai1* and *Ovol2* observed in the present study may reflect a transcriptional adaptation associated with epithelial plasticity and cellular states relevant to regenerative competence. This interpretation is further supported by the concomitant enhancement of cellular migration and metabolic activity, indicating that the transcriptional

changes associated with epithelial plasticity occur alongside functional responses relevant to regenerative competence.

Collectively, the findings indicate that selected He-PAM conditions induce coordinated functional and transcriptional responses associated with stem/progenitor activation, migratory competence, and epithelial plasticity. This integrated response is consistent with current models of HFSC regulation, in which regenerative competence depends on coordinated changes in stem-cell activity and cellular state rather than on a single molecular or functional endpoint [9, 11, 33–36]. Further studies incorporating direct characterization of signaling pathways and PAM chemistry, together with follicular ex vivo and in vivo models, will be required to determine the mechanistic and regenerative significance of these responses.

Several limitations should be considered when interpreting these findings. The present study was designed as a functional and transcriptional investigation and therefore does not establish causal activation of specific signaling pathways. Accordingly, the proposed involvement of Wnt/β-catenin-related regulation, CXCR4-associated migratory signaling, and epithelial–mesenchymal plasticity should be regarded as a biologically supported framework derived from the combined functional and gene-expression data rather than as a demonstrated molecular mechanism. In addition, the reactive-species composition of He-PAM was not directly quantified; therefore, the observed cellular responses cannot be attributed to individual plasma-generated reactive species or to a defined redox dose. The experiments were performed in vitro and did not directly assess hair-cycle re-entry or follicular regeneration in vivo. Finally, the cell population investigated in this study was isolated using the established rat vibrissal bulge-explant approach described in Section 2.2, and Nestin expression was confirmed in the present cultures. However, because the hair-follicle bulge contains heterogeneous stem/progenitor populations and a broader lineage-specific marker panel was not examined in the present experiments, the findings should be interpreted specifically in the context of this nestin-expressing, bulge-derived stem/progenitor population. Future studies combining pathway-specific perturbation and signaling analyses with characterization of PAM chemistry, broader phenotypic characterization of the bulge-derived cell population, and follicular ex vivo or in vivo models will be required to define the molecular determinants of the He-PAM response and determine whether the regeneration-associated cellular responses observed here translate into enhanced follicular regeneration. Although cells were obtained from nine rats through three independent isolation procedures, the resulting cell populations were pooled before the experimental assays. Consequently, the three experimental runs were performed using a shared cell population rather than independently derived biological replicates. This design did not allow assessment of donor-to-donor or isolation-to-isolation variability, which should be addressed in future studies using independently maintained cell preparations.

5. Conclusion

Selected He-PAM treatment enhanced HFSC metabolic activity and migration and induced coordinated transcriptional changes in genes associated with regenerative activation (*Runx1*, *Lgr4*, and *Ccnd1*),

migratory responsiveness (*Cxcr4*), and epithelial plasticity (*Snai1* and *Ovol2*). The convergence of these functional and transcriptional responses indicates that He-PAM can modulate multiple cellular processes relevant to regenerative competence rather than acting through a single cellular endpoint.

Collectively, these findings define a regeneration-associated response to He-PAM and provide a rationale for further investigating plasma-activated media as a strategy for modulating cellular processes relevant to hair follicle regeneration. Because the present study was conducted in vitro and did not directly assess hair-cycle activation or follicular regeneration, validation in follicular ex vivo and in vivo models will be required to determine whether these cellular responses translate into regenerative outcomes.

Declarations

Use of artificial intelligence

During the preparation of this work, the authors used ChatGPT in order to improve language and readability. After using this tool, the authors reviewed and edited the content as needed and take full responsibility for the content of the published article.

Clinical trial number

not applicable.

Ethics approval and consent to participate

No live animals were used specifically for this study. The animals had originally been bred and used for other research projects unrelated to the present study. The animals used as the source of the post-mortem tissues were from the approved project entitled “Investigating the effect of platelet-rich plasma-derived nanovesicles activated by jet plasma on damage induced by bleomycin in Wistar rat testicular cells,” approved by the Research Ethics Committees of Kharazmi University (Approval ID: IR.KHU.REC.1404.027; Approval Date: May 25, 2025). Following euthanasia, otherwise unused post-mortem tissues, including whisker-pad tissues, were collected for the isolation of hair follicle stem cells for the present study. This approach avoided the use of additional animals and was consistent with the principles of the 3Rs (Replacement, Reduction, and Refinement).

Funding:

This work has been supported by Center for International Scientific Studies & Collaborations (CISSC), Ministry of Science Research and Technology of Iran, research grant 4020466.

Author Contribution

S.E. performed the experiments, analyzed the data, prepared the figures, and wrote the original manuscript. K.H. conceived and designed the study, supervised the research, interpreted the results, and critically revised the manuscript. E.H. contributed to the study conception, supervision, and manuscript revision. H.M. contributed to scientific supervision and manuscript review. S.P., E.T. and E.R. contributed to scientific interpretation and manuscript revision. All authors reviewed and approved the manuscript.

Acknowledgement

The authors gratefully acknowledge Kavosh Biotech Company for its assistance with real-time PCR analyses.

Data Availability

All data supporting the findings of this study are available within the paper .

References

1. Ahmadi, S. et al. Enhanced neural differentiation of epidermal neural crest stem cell by synergistic effect of lithium carbonate and crocin on BDNF and GDNF expression as neurotrophic factors. *Iran. J. Pharm. Research: IJPR*. **20** (2), 95 (2021).
2. Xing, Y. Z. et al. Recent progress in hair follicle stem cell markers and their regulatory roles. *World J. stem cells*. **16** (2), 126 (2024).
3. Chew, M. W. et al. *Hair follicle inspired therapies for wound healing and scar remodelling* (Journal of Plastic, Reconstructive & Aesthetic Surgery, 2025).
4. Ito, M. et al. Stem cells in the hair follicle bulge contribute to wound repair but not to homeostasis of the epidermis. *Nat. Med.* **11** (12), 1351–1354 (2005).
5. Pandamooz, S. et al. The influence of cerebrospinal fluid on epidermal neural crest stem cells may pave the path for cell-based therapy. *Stem Cell Res. Ther.* **4** (4), 84 (2013).
6. Lee, J. H. & Choi, S. Deciphering the molecular mechanisms of stem cell dynamics in hair follicle regeneration. *Exp. Mol. Med.* **56** (1), 110–117 (2024).
7. Zhang, B. & Chen, T. Local and systemic mechanisms that control the hair follicle stem cell niche. *Nat. Rev. Mol. Cell Biol.* **25** (2), 87–100 (2024).
8. Zou, X. et al. TWEAK regulates the functions of hair follicle stem cells via the Fn14-Wnt/β-catenin-CXCR4 signalling axis. *Wound Repair. Regeneration*. **33** (3), e70032 (2025).
9. Lamouille, S., Xu, J. & Derynck, R. Molecular mechanisms of epithelial–mesenchymal transition. *Nat. Rev. Mol. Cell Biol.* **15** (3), 178–196 (2014).

10. Nieto, M. A. et al. EMT: 2016. *cell* **166** (1), 21–45 (2016).
11. Watanabe, K. et al. OVOL2 induces mesenchymal-to-epithelial transition in fibroblasts and enhances cell-state reprogramming towards epithelial lineages. *Sci. Rep.* **9** (1), 6490 (2019).
12. Hahn, O. et al. Cold atmospheric pressure plasma-activated medium modulates cellular functions of human mesenchymal stem/stromal cells in vitro. *Int. J. Mol. Sci.* **25** (9), 4944 (2024).
13. Schmidt, A. & Bekeschus, S. Redox for repair: cold physical plasmas and Nrf2 signaling promoting wound healing. *Antioxidants* **7** (10), 146 (2018).
14. Robert, E. et al. State of the Art on the Understanding of Plasma Jet Interaction with Skin Tissue Models. *Plasma Med.*, **15**(1). (2025).
15. Labérie, B., Saugé, L., Polesskaya, A., Rousseau, A. & Gautreau, A. M. Cold atmospheric plasma promotes migration persistence, through induced H_2O_2 and electric field. *Biophys. J.* **125** (3), 697–708 (2026).
16. Wu, P. S. et al. Cold Atmospheric Plasma Jet Promotes Wound Healing Through CK2-Coordinated PI3K/AKT and MAPK Signaling Pathways. *Mol. Cell. Proteom.* **24** (5), 100962 (2025).
17. Roux, S., Marchès, A., Galiacy, S., Merbahi, N. & Simon, M. Biological solutions activated by cold plasma at atmospheric pressure: A new therapeutic approach for skin wound healing. *Biomed. Pharmacother.* **186**, 118001 (2025).
18. Wang, P. et al. Epithelial-to-mesenchymal transition enhances cancer cell sensitivity to cytotoxic effects of cold atmospheric plasmas in breast and bladder cancer systems. *Cancers* **13** (12), 2889 (2021).
19. Chen, M., Chen, J., Xie, T., Chen, Z. & Xu, G. Effects of cold atmospheric plasma-treated medium on HaCaT and HUVEC cells in vitro. *Plasma Processes Polym.* **21** (11), e2400132 (2024).
20. Hoi, C. S. et al. Runx1 directly promotes proliferation of hair follicle stem cells and epithelial tumor formation in mouse skin. *Mol. Cell. Biol.* **30** (10), 2518–2536 (2010).
21. Hwang, J. H. et al. Non-thermal atmospheric pressure plasma activates Wnt/β-catenin signaling in dermal papilla cells. *Sci. Rep.* **11** (1), 16125 (2021).
22. Ren, X. et al. Lgr4 deletion delays the hair cycle and inhibits the activation of hair follicle stem cells. *J. Invest. Dermatology*. **140** (9), 1706–1712 (2020). e4.
23. Blaise, O. et al. Infected wound repair correlates with collagen I induction and NOX2 activation by cold atmospheric plasma. *npj Regenerative Med.* **9** (1), 28 (2024).
24. Mongkolpobsin, K. et al. Cold atmospheric microwave plasma (CAMP) stimulates dermal papilla cell proliferation by inducing β-catenin signaling. *Sci. Rep.* **13** (1), 3089 (2023).
25. Mousavi, S. M. et al. Therapeutic potential of hair follicle-derived stem cell intranasal transplantation in a rat model of ischemic stroke. *BMC Neurosci.* **23** (1), 47 (2022).
26. Pandamooz, S. et al. Directing Rat Hair Follicle Stem Cells Toward Neuronal Lineage With Enhanced Trophic Factor Expression. *Adv. Biomedical Res.* **13**, 84 (2024).

27. Osorio, K. M., Lilja, K. C. & Tumbar, T. Runx1 modulates adult hair follicle stem cell emergence and maintenance from distinct embryonic skin compartments. *J. Cell Biol.* **193** (1), 235–250 (2011).
28. Choi, Y. S. et al. Distinct functions for Wnt/β-catenin in hair follicle stem cell proliferation and survival and interfollicular epidermal homeostasis. *Cell. stem cell.* **13** (6), 720–733 (2013).
29. Xu, X., Lyle, S., Liu, Y., Solky, B. & Cotsarelis, G. Differential expression of cyclin D1 in the human hair follicle. *Am. J. Pathol.* **163** (3), 969–978 (2003).
30. Bekeschus, S., von Woedtke, T., Emmert, S. & Schmidt, A. Medical gas plasma-stimulated wound healing: Evidence and mechanisms. *Redox Biol.* **46**, 102116 (2021).
31. Chuang, K. T., Chiou, S. S. & Hsu, S. H. Recent advances in transcription factors biomarkers and targeted therapies focusing on epithelial–mesenchymal transition. *Cancers* **15** (13), 3338 (2023).
32. Zhang, L. et al. SNAI1 promotes epithelial-mesenchymal transition and maintains cancer stem cell-like properties in thymic epithelial tumors through the PIK3R2/p-EphA2 Axis. *J. Experimental Clin. Cancer Res.* **43** (1), 324 (2024).
33. Jimenez-Castaño, R. & Nieto, M. A. *Epithelial-to-mesenchymal transition as a central driver of tumor cell plasticity*. *Nat. Cancer*, : pp. 1–16. (2026).
34. Ji, S. et al. Functional hair follicle regeneration: an updated review. *Signal. Transduct. Target. Therapy*. **6** (1), 66 (2021).
35. Mao, M. Q. et al. Epithelial-mesenchymal interaction in hair regeneration and skin wound healing. *Front. Med.* **9**, 863786 (2022).
36. Solanas, G. & Benitah, S. A. Regenerating the skin: a task for the heterogeneous stem cell pool and surrounding niche. *Nat. Rev. Mol. Cell Biol.* **14** (11), 737–748 (2013).

Figures

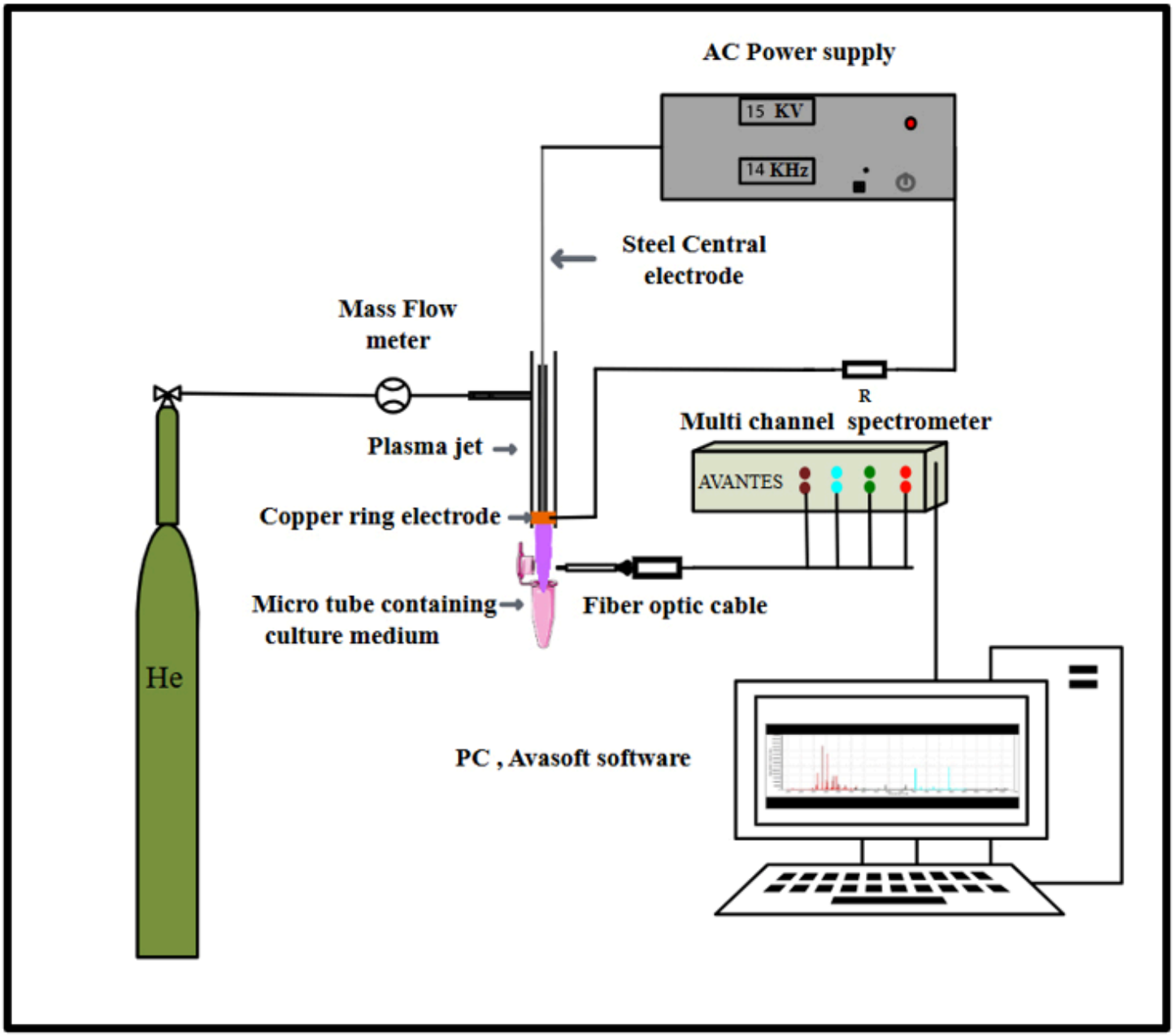

Figure 1

Schematic of helium CAP jet setup for PAM generation.

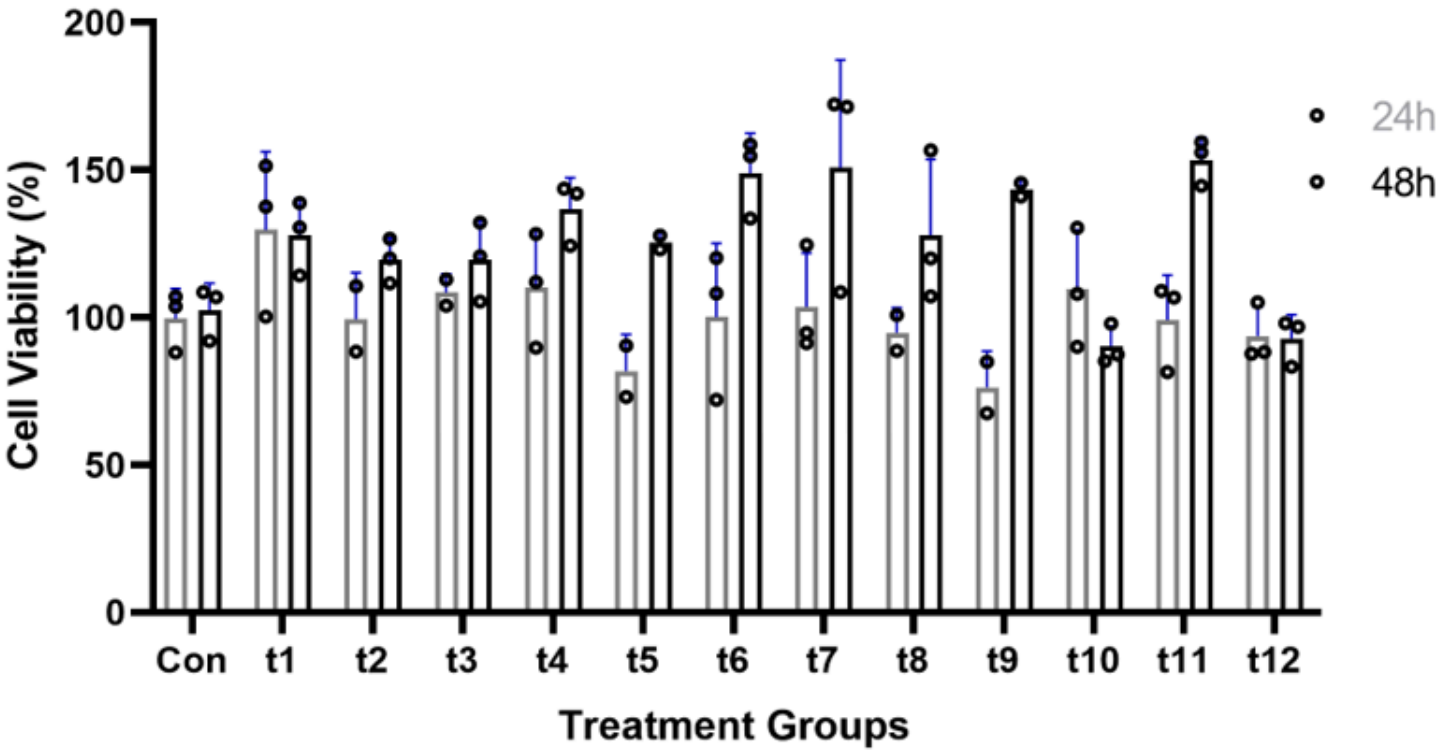

Figure 4

Metabolic activity of HFSCs at 24 and 48 h following treatment with He-PAM generated under different plasma conditions. Data are presented as mean ± SD from three separate experimental runs using the shared cell population (n = 3 experimental runs). Statistical comparisons were performed between each treatment group and the corresponding time-matched control (*p < 0.05, **p < 0.01, ***p < 0.001).

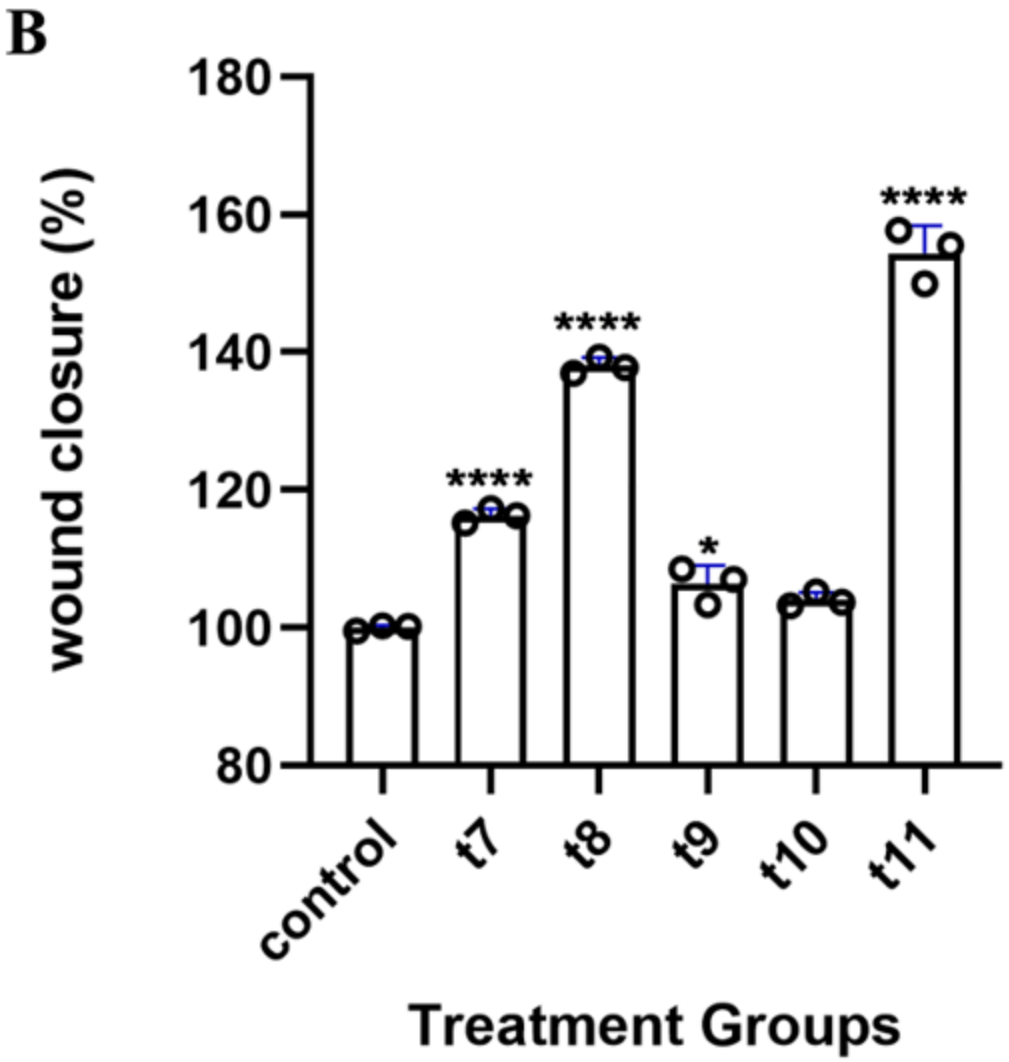

Figure 5

Effect of He-PAM on the migratory response of HFSCs. (A) Representative scratch-assay images of untreated control cells at 0 and 48 h and He-PAM-treated cells at 48 h. (B) Quantitative analysis of relative wound closure normalized to the untreated control (control = 100%). The actual wound-closure percentages were 59.8% for the control, 82.6% for t8, and 92.4% for t11, corresponding to approximately 138% and 155% of the control for t8 and t11, respectively. Data are presented as mean ± SD from three separate experimental runs using the shared cell population (n = 3 experimental runs). Statistical significance versus the control group is indicated by *p < 0.05, **p < 0.01, ***p < 0.001, and ****p < 0.0001.

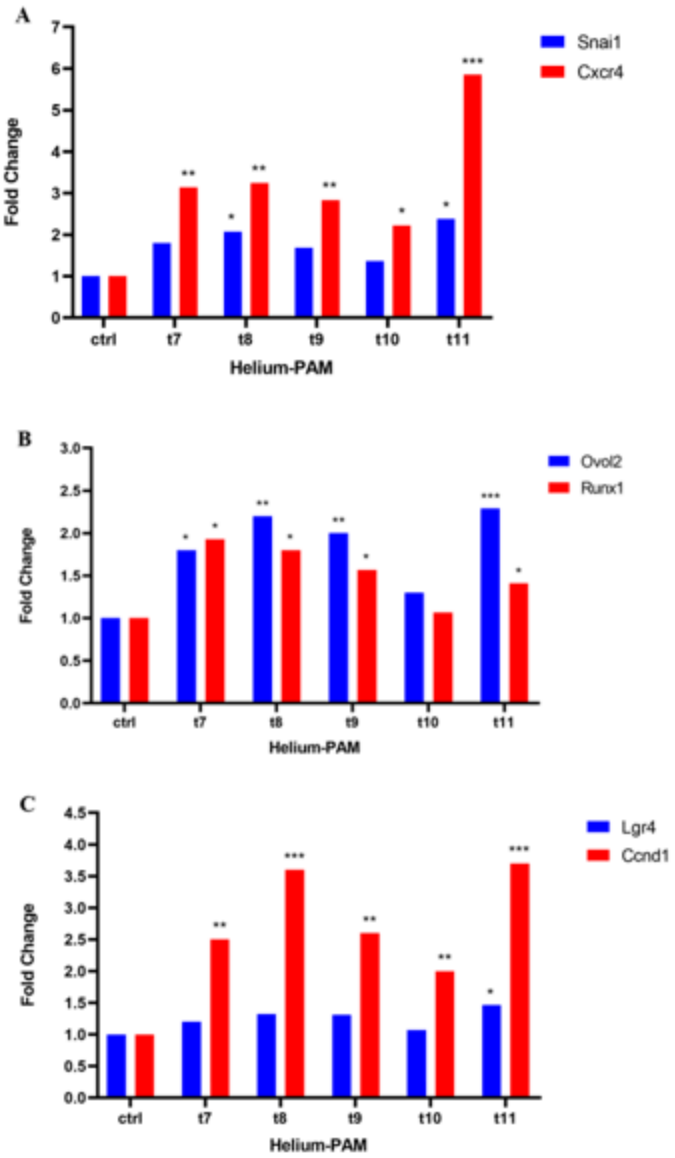

Figure 6

Relative fold changes in *Snai1*, *Cxcr4, Ovol2, Runx1, Lgr4,*and *Ccnd1* expression 48 h after He-PAM treatment. Asterisks indicate statistically significant differences between He-PAM-treated and control groups ($p < 0.05$, **p** < 0.01, ***p***< 0.001).